

Operation of graphene quantum Hall resistance standard in a cryogen-free table-top system

T.J.B.M. Janssen¹, S. Rozhko¹, I. Antonov², A. Tzalenchuk^{1,2},
J.M. Williams¹, Z. Melhem,³ H. He⁴, S. Lara-Avila⁴, S.
Kubatkin⁴, R. Yakimova⁵

¹National Physical Laboratory, Hampton Road, Teddington TW11 0LW, UK

²Royal Holloway, University of London, Egham TW20 0EX, UK

³Oxford Instruments Nanoscience, Tubney Woods, Abingdon OX13 5QX, UK

⁴Department of Microtechnology and Nanoscience, Chalmers University of Technology, S-41296 Göteborg, Sweden

⁵Department of Physics, Chemistry and Biology (IFM), Linköping University, S-58183 Linköping, Sweden

E-mail: jt.janssen@npl.co.uk

Abstract. We demonstrate quantum Hall resistance measurements with metrological accuracy in a small cryogen-free system operating at a temperature of around 3.8 K and magnetic fields below 5 T. Operating this system requires little experimental knowledge or laboratory infrastructure, thereby greatly advancing the proliferation of primary quantum standards for precision electrical metrology. This significant advance in technology has come about as a result of the unique properties of epitaxial graphene on SiC.

1. Introduction

One of the goals of the modern-day metrology is to provide quantum standards at the fingertips of the end-users, shortening the calibration chain from primary standards to the final product. A shorter calibration chain will result in a higher accuracy for end-users which can be exploited to develop more advanced test and measurement equipment and subsequently lead to societal benefits where measurement is an issue.

Resistance metrology is one of the cornerstones of electrical metrology with most national measurements laboratories around the world providing an extensive range of calibration services across many decades of resistance value [1]. The primary standard for resistance is based on the quantum Hall effect (QHE) [2] which is presently realised by a lot fewer laboratories [3]. This is because the infrastructure needed to create the QHE in conventional semiconductor systems is quite elaborate and expensive as it requires temperatures of 1 K or below and magnetic fields around 10 T. Another important barrier is the expertise needed to run a quantum Hall system and verify the correct operation and quantisation parameters. Finally, liquid Helium is becoming a scarce resource, significantly increasing in price year on year, and not readily available in every country.

A simpler, cryogen-free, system is needed if more laboratories are to realise the primary standard directly and this has recently become possible with the advent of graphene. One of the first properties observed in graphene was the QHE and it was immediately realised that it is ideal for metrology by virtue of its unique band structure [4, 5, 6, 7]. The Landau level quantisation in graphene is a lot stronger than in traditional semiconductor systems which implies that both a lower magnetic field can be used and that the low temperature constraint is more relaxed [6]. Following the original demonstration of high-accuracy quantum Hall resistance measurements in epitaxial graphene grown on SiC [8] and proof of the universality of the QHE between graphene and GaAs [9], recently these results have been very nicely reproduced by a number of different research groups [10, 11, 12]. Particularly, a recent publication by the LNE group has demonstrated that ppb-accuracy can be achieved over a large experimental parameter range [12]. These results also demonstrate that devices which show extraordinary good quantum Hall effect at high magnetic field and low temperature are not necessarily optimum for low magnetic field and high temperature measurements.

Measurements of the QHE at low magnetic field are complicated by the fact that the carrier density needs to be reduced to a level well below the as-grown density of epitaxial graphene on SiC [13] (SiC/G). Unlike exfoliated graphene on SiO₂, gating of graphene on SiC is not straightforward [14, 15, 16]. Recently, a novel technique was demonstrated which creates a static top-gate by depositing ions via corona discharge [17]. This technique allows for a systematic control of the carrier density and both n and p -type densities can be achieved on both sides of the Dirac point. Importantly this method is fully reversible and can be applied repeatably. Another issue with low carrier density graphene is the homogeneity. Under these conditions it is well known that electron-hole

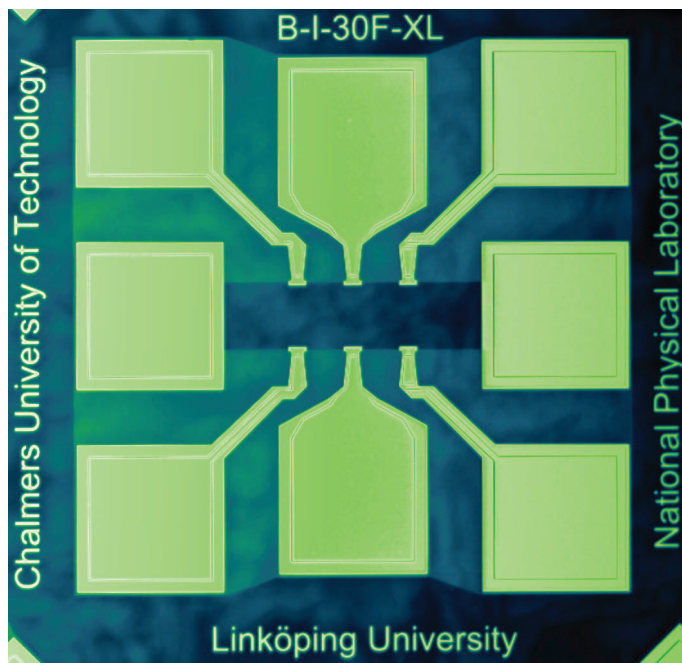


Figure 1. Optical microscope image of a typical device used in our experiments (not the one used for the actual experiments). The channel width is $100\ \mu\text{m}$, dark area is graphene channel, light area is SiC substrate and gold are the metallic contact.

puddles form [18] induced by charged impurities, however, in epitaxial graphene the disorder strength can be of order $10\ \text{meV}$, comparable to flakes on boron-nitride [19].

Here we demonstrate for the first time measurements of the QHE with part-per-billion (ppb)-accuracy in a small table-top cryogen-free pulse-tube system. Both the longitudinal resistivity R_{xx} and the contact resistance R_c were well within the limits set by the QHR guidelines [20]. Using corona gating the carrier density was controlled such that the maximum breakdown current occurred just below the maximum magnetic field of our system. The noise sources in the system were reduced to a level such that the overall standard deviation of the measurements was comparable to those achieved for a conventional liquid $^4\text{He}/^3\text{He}$ system. The system is extremely easy to operate (it has only one button) and can run unattended for months on end, providing a stable and primary resistance reference whenever and wherever it is needed.

2. Device design and fabrication

Graphene was grown on the Si-face of SiC at $T = 2000\ ^\circ\text{C}$ and $P = 1\ \text{atm}$ Ar (GraphenSIC AB) [21]. In total 20 Hall bars of different dimensions (30 and $100\ \mu\text{m}$ wide channels) and voltage probe types were patterned on the SiC/G using standard electron-beam lithography, lift-off, and oxygen plasma etching, as reported elsewhere [22]. The Hall bars are oriented parallel or perpendicular with respect to the predominant step edge direction of the SiC substrate. The sample was spin-coated with a thin, $100\ \text{nm}$,

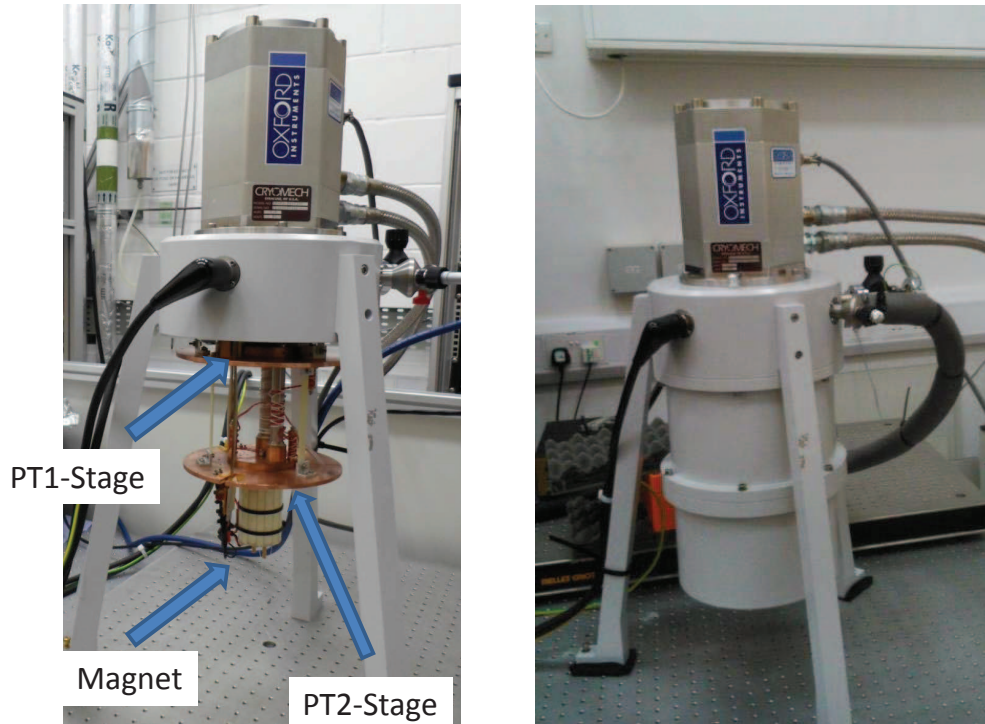


Figure 2. a) Inside of the cryostat cooler showing the small superconducting magnet, mounted at the bottom of the PT2 Stage. b) The system with vacuum can mounted. The overall height of the system is around 80 cm.

layer of poly(methyl methacrylate-co-methacrylate acid), henceforth P(MMA-MAA) (MicroChem Corp., PMMA copolymer resist solids 6% in ethyl lactate).

All results presented in this paper are measured on a Hall bar with a $30 \mu\text{m}$ wide and $180 \mu\text{m}$ long channel. A comprehensive study of all devices on this chip will be presented at a later date.

3. The measurement system

The measurement system for primary resistance consists of two parts, the quantum Hall system and the measurement bridge.

3.1. Table-top cryogen-free QHR cryostat

Today, cryogen-free superconducting magnet systems have become omnipresent in low temperature physics laboratories because of their ease-of-use and reduced operational cost. In particular, for low magnet fields, $\leq 5 \text{ T}$, these systems can be very small and simple. The 5 T superconducting magnet in our system is only 7.5 cm tall with an outer diameter of 6 cm. The inductance is 0.5 H and is small enough to be cooled by a 0.25 W pulse-tube cooler (see Fig. 2). The bore of this magnet is 3 cm in diameter which is large enough to take a standard TO8 header used in QHR metrology. The system has high- T_C current

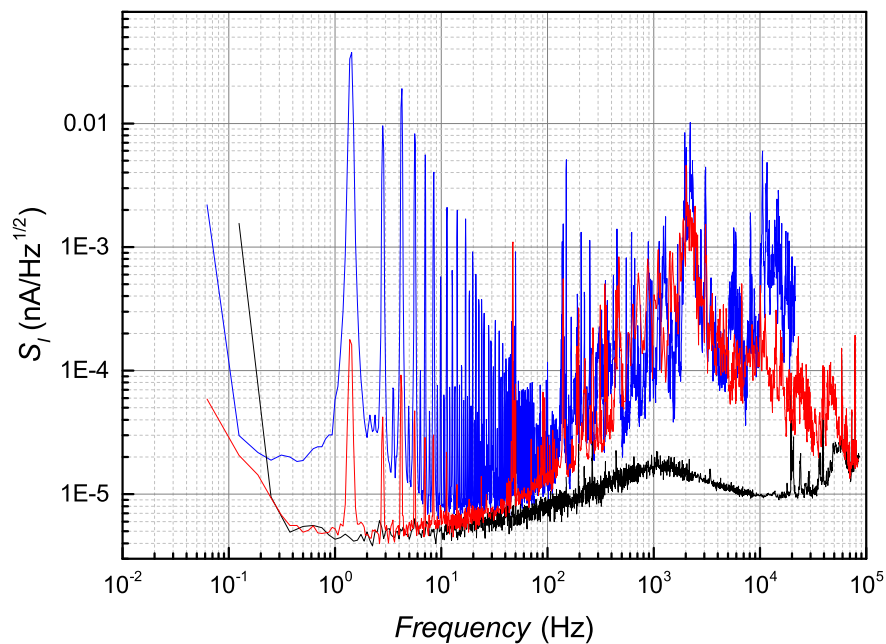


Figure 3. Current noise measurement traces before (blue) and after (red) modification of the pulse-tube cryostat. The black trace was measured with the pulse-tube compressor switched off. Current noise was measured on the sample wires without a sample present.

leads for the magnet which requires ~ 60 A for full field. After evacuation the system cools down in approximately 5 hours from room temperature to ~ 3.8 K.

In a cryogen-free system there are a number of noise sources not normally present in a traditional wet system. There is the compressor which produces the high-pressure helium gas and the rotating valve and stepper motor on top of the cryostat. These sources of noise need to be controlled and reduced as much as possible so as to not compromise the sensitivity of the measurement system. The noise of the compressor can simply be reduced by either placing an acoustic box around it or locating it in an adjoining space on the other side of a separating wall. Recently, a new type of high pressure hose was developed which significantly reduces the high-pitched hiss. These so-called quiet hoses have two beneficial effects, firstly it significantly reduces the vibrations in the cryostat system and secondly it is much more pleasant for the operator. Another improvement has been to replace the standard pulsed drive unit for the stepper motor with a low noise linear drive system. A number of other modifications are, plastic isolators on the high pressure lines to galvanically isolate the compressor from the cryostat and filters on the magnet current leads. Inside the cryostat care has to be taken that the experimental wiring is as tightly fixed as possible to reduce the effect of vibrations. Also the measurement wiring requires good heat sinking because these are

relatively short compared to traditional wet systems.

The corollary of these improvements can be seen in the noise traces in Fig. 3. The traces are measured on the sample wires with a spectrum analyser before and after the modifications. A reference trace with the compressor switched off is also shown. We can see that the low frequency noise peaks are reduced by more than two orders of magnitude and noise floor is equal to that measured with the compressor switched off. The higher frequency noise is largely unaffected by the modifications but this noise is outside the CCC measurement bandwidth and is not critical.

3.2. The cryogenic current comparator bridge

High accuracy measurements of resistance ratios are generally made using a so-called cryogenic current comparator (CCC) bridge. The fully automated CCC bridge used in our experiments has been described in great detail before [23, 24]. In a CCC bridge, currents are locked in the inverse ratio of the resistances being compared. A CCC establishes the current ratio by passing the currents along wires through a superconducting tube and measuring the residual screening current on the outside of the tube with a superconducting quantum interference device (SQUID). The difference between the voltages developed across the resistors is measured using a sensitive voltmeter and allows one resistor to be determined with respect to the other. In primary resistance metrology one of the resistors is a quantum Hall device with a resistance value exactly equal of $R_H = R_K/i$ where $R_K = h/e^2$, e is the elementary charge, h is the Planck constant and i is an integer and generally $i = 2$ or 4 is used for semiconductor devices. In graphene, owing to the bandstructure, only $i = 2$ is available. The maximum achievable sensitivity of the bridge depends for a large part on the signal-to-noise ratio in the voltmeter and therefore on the maximum current used to drive the resistors (the Johnson noise in the resistors is the other limiting factor) [23]. Under optimum conditions measurement accuracies in excess of 1 part in 10^{10} can be achieved [9, 25]. However, for routine resistance metrology a few parts in 10^9 in a reasonable measurement time (~ 15 min) is perfectly adequate. In the present system the cryogenic environment needed for the superconducting tube and SQUID is provided by a traditional liquid helium cryostat.

4. Characterisation

Fig. 4 shows an example measurement of R_{xx} and R_{xy} made at the base-temperature of 3.8 K in the cryogen-free system described in the previous section. The curves display the familiar shape characteristic for epitaxial graphene on SiC which has been observed many times before [26, 27, 14, 8, 28, 10, 12]. The carrier density was reduced to $5.4 \times 10^{10} \text{cm}^{-2}$ by corona-gating from the as grown density of $n \approx 10^{13} \text{cm}^{-2}$. A wide plateau in R_{xy} is observed whilst R_{xx} is zero. The width of the plateau is much larger than would be expected from the low field carrier density. This behaviour is explained in

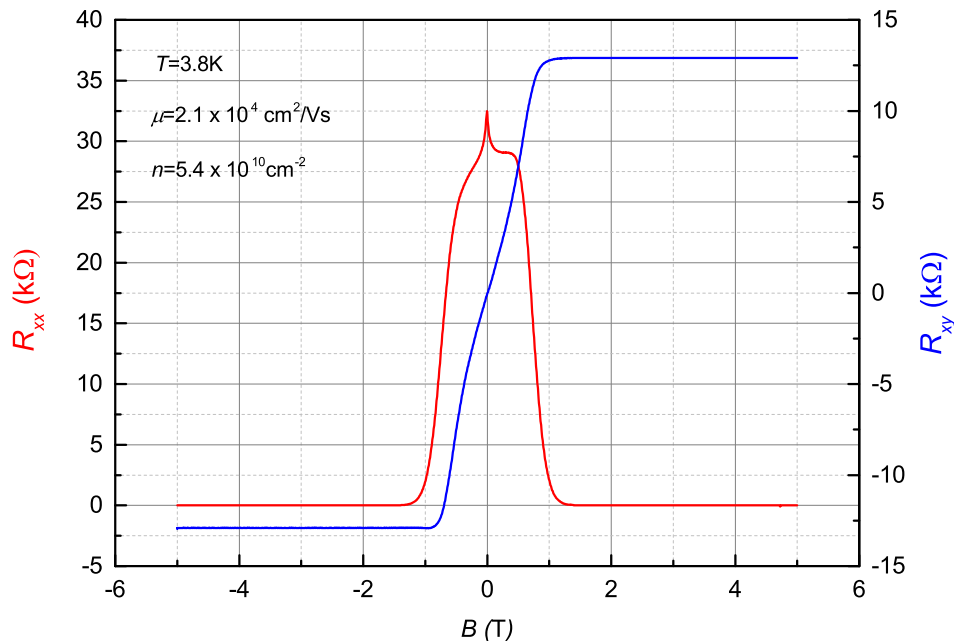


Figure 4. R_{xx} (Red) and R_{xy} (Blue) on an epitaxial graphene Hall bar device measured at 3.8 K in the cryogen-free cryostat, measured with a source-drain current of $I_{sd} = 100$ nA.

terms of a magnetic field driven charge transfer from the interface layer to the graphene layer which results in an increase in carrier density as the magnetic field increases and effectively pins the Fermi level at exact filling of $\nu = 2$ [13, 28].

When attempting to make accurate quantum Hall resistance measurements the first step is to properly characterise the sample according to guidelines set out for primary resistance metrology [20]. Key parameters are the longitudinal resistance (R_{xx}) and contact resistance (R_c) at the desired measurement current. The longitudinal resistance needs to be as low as possible and preferably below a few tens of $\mu\Omega$ and checked on both sides of the device. Often these measurements are limited by the resolution of the nanovoltmeter and other methods can be employed to verify accurate quantisation [20]. The contact resistance can be accurately determined using a three terminal measurement technique in the quantised Hall state. This method determines $R_c + R_l$ where R_c is the contact resistance and $R_l = 6.4 \Omega$ is the lead resistance in the cryostat in our system. For our device we find R_c between 0.1 and 1 Ω for all contacts measured with a current of $10\mu\text{A}$.

The optimum conditions for QHR measurements are easiest to obtain when the breakdown current is maximum and significantly larger than the source-drain measurement current, I_{sd} . Here the breakdown current is defined as the maximum source-drain current the device can sustain before a measurable longitudinal resistance

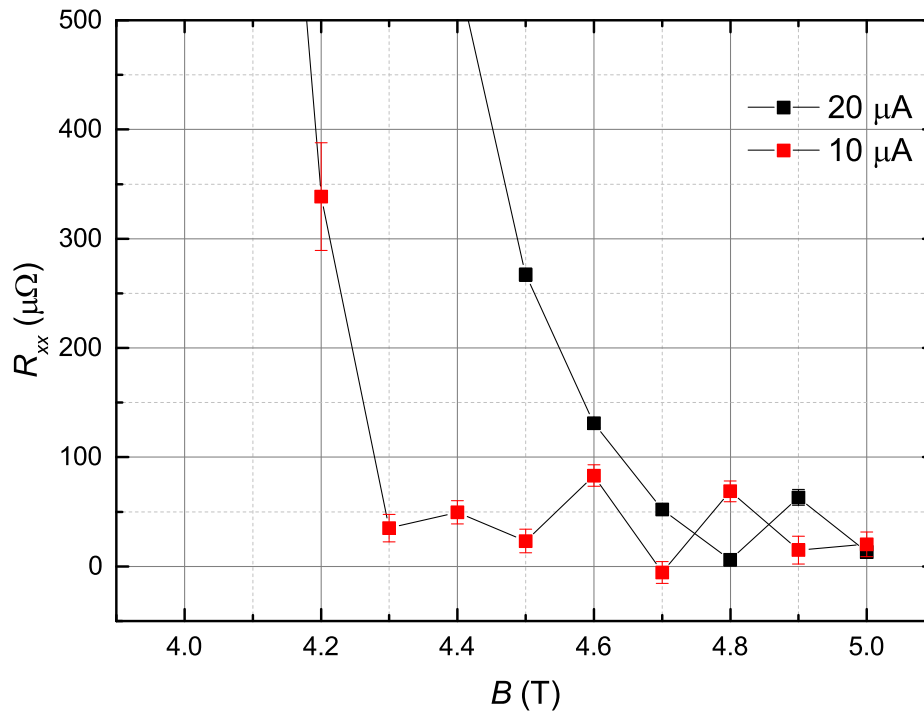
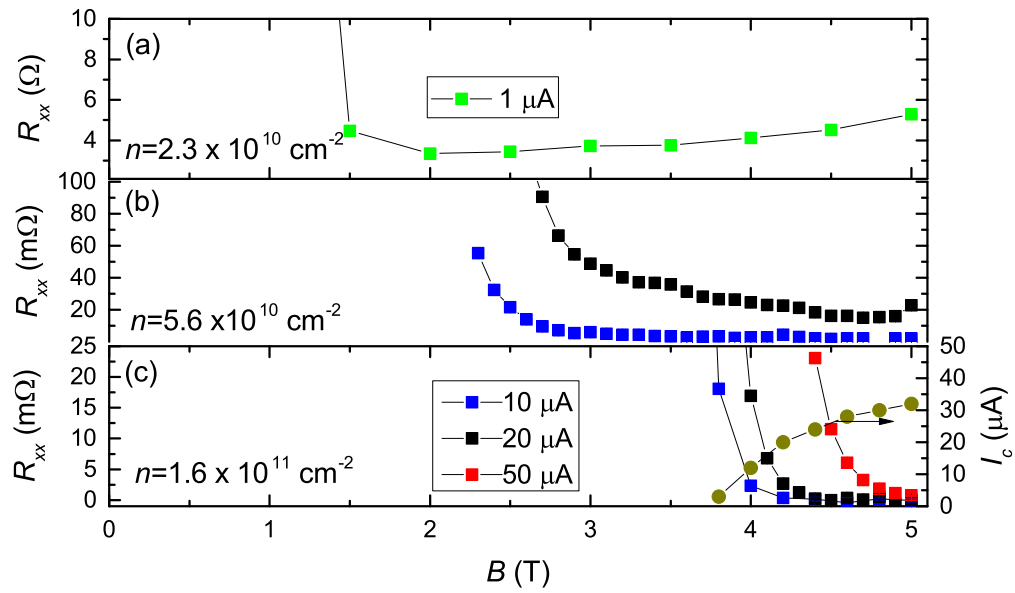


Figure 5. Top graph: R_{xx} as a function of magnetic field for different charge carrier densities. Temperature is $\approx 3.8 \text{ K}$. Plot (c) also shows the breakdown current I_C as a function of magnetic field. Bottom graph: high-resolution measurement of R_{xx} in a 1 T magnetic field range for $n = 1.6 \times 10^{11} \text{ cm}^{-2}$. This resolution was obtained by repeated measurements (typically 50 to 100) of V_{xx} with positive and negative I_{sd} .

appears ‡. For higher carrier density devices, the breakdown current tends to be higher because the $\nu = 2$ state occurs at a higher magnetic field [29] which is simply related to the fact that at higher magnetic field, the Landau levels are further apart and hence the quantisation is stronger [29]. For epitaxial graphene I_{sd} was shown to follow a $\propto B^{3/2}$ behaviour similar to that observed in semiconductor systems [30].

This effect poses a particular problem for optimising the carrier density for accurate QHR measurements at the low magnetic fields available in our small cryogen-free system. If the carrier density is too low the maximum in the breakdown current will occur at a very low magnetic field and its value will be equally low. Fig. 5a shows a measurement of R_{xx} at a $n = 2.3 \times 10^{10} \text{ cm}^{-2}$ very close to the Dirac point. For a $I_{sd} = 1 \text{ } \mu\text{A}$ we find that the longitudinal resistance is always larger than a few Ohms and consequently the device is not properly quantised. Fig. 5b shows R_{xx} at a $n = 5.6 \times 10^{10} \text{ cm}^{-2}$ and we can observe proper quantisation in a 2 T-range for $I_{sd} = 10 \text{ } \mu\text{A}$ but for $I_{sd} = 20 \text{ } \mu\text{A}$, R_{xx} is in the $m\Omega$ range and the device becomes unquantised (see below). When the carrier density is set even higher (see Fig. 5c), quantisation becomes stronger but the usable magnetic field range shrinks to around 0.5 T. The bottom graph in Fig. 5 shows a high-resolution measurement of R_{xx} in this range demonstrating longitudinal resistance of order $10 \text{ } \mu\Omega$ and confirming proper quantisation.

Using the magnetic field dependent charge-transfer model it is straightforward to estimate the optimum charge carrier density for maximum breakdown current [28]. Assuming that the maximum breakdown current will occur when $\nu = 2$ filling factor coincides with our maximum magnetic field of 5 T [29], gives a carrier density of $\approx 2.4 \times 10^{11} \text{ cm}^{-2}$. Setting this density as n_∞ in the model calculation of Ref. [28] allows us to obtain the zero field carrier density. $n_\infty = \frac{A\gamma}{1+e^2\gamma/c_c} - n_g$ in which A is the difference in work function between graphene and the donor states in SiC, γ is the density of donor states, c_c is the classical capacitance and n_g is the deposited corona gate charge. Using γ as a fit parameter we obtain a value for the optimum carrier density of $n_S \approx 1.3 \times 10^{11} \text{ cm}^{-2}$ (see Fig. 6).

Figure 7 shows the measured maximum breakdown current measured at $B = 5 \text{ T}$ as a function of zero field charge carrier density for two sets of data 3 months apart. The graph confirms that optimum carrier density is around $n_S = 1.3 \times 10^{11} \text{ cm}^{-2}$. For the later data set the breakdown current was almost half the original breakdown current which could be related to the degradation of one of the current contacts on the device. The cause of this degradation is yet unclear and needs to be investigated further because QHR devices for quantum resistance metrology need to be stable and reproducible over long periods of time. The original maximum breakdown current is $60 \text{ } \mu\text{A}$ which for our channel width of $30 \text{ } \mu\text{m}$ implies a current density of 2 Am^{-1} density which is close to the theoretical maximum [29].

‡ We typically use a limit of 10 nV for V_{xx} which for $I_{sd} = 10 \text{ } \mu\text{A}$ would imply a $R_{xx} = 1 \text{ m}\Omega$

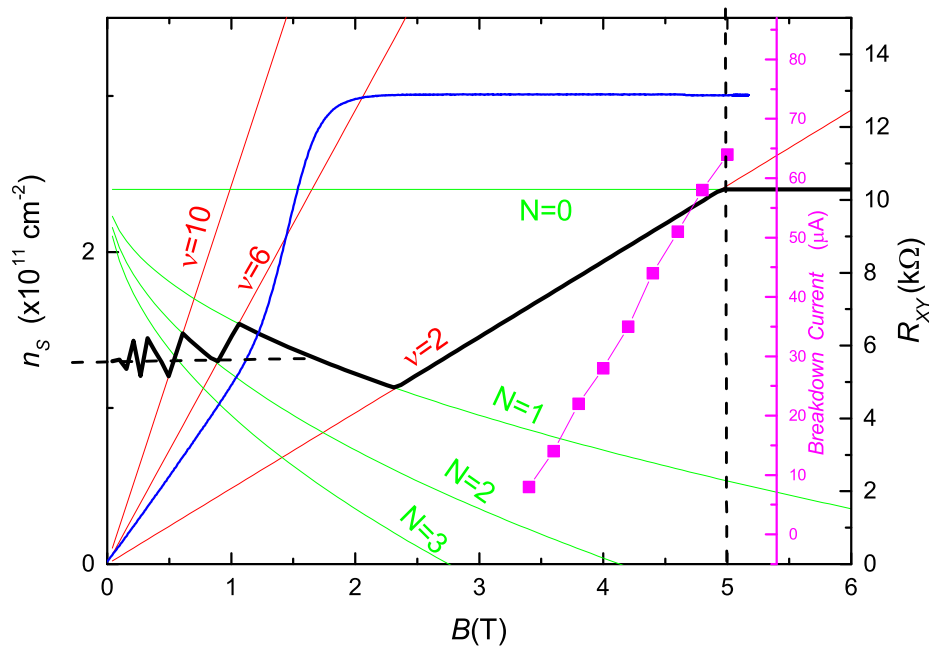


Figure 6. n_s versus magnetic field using the model from Ref. [28] (thick black line). Red lines are constant filling factors and green lines are $n_s(B, N)$. Blue line is R_{XY} measured for a device with $n_s \approx 1.3 \times 10^{11} \text{ cm}^{-2}$ (right hand axis) together with the measured breakdown current (purple squares and second purple right hand axis). Vertical dashed line indicates maximum magnetic field of 5 T and horizontal dashed line indicates zero field carrier density of $1.3 \times 10^{11} \text{ cm}^{-2}$.

5. Quantum Hall resistance measurements

Figure 8 shows the central result of this paper. Here we measured the quantum Hall resistance in terms of a nominally 100Ω temperature controlled standard resistor using the CCC bridge. The data in Fig. 8 is normalised to the mean value of the resistor since we are not concerned with the absolute accuracy of the QHE in graphene which was established earlier [9]. The measurements are made at two different source-drain currents (≈ 10 and $\approx 20 \mu\text{A}$) as a function of magnetic field. Comparing the data for $10 \mu\text{A}$ with that for $20 \mu\text{A}$ it is clear that for the larger measurement current, the device is not properly quantised. This fact is also confirmed by the measurement of R_{xx} which show a significant deviation from zero for this larger current. The low breakdown current is not a major issue because the sample chip contains a number of devices with a larger width ($100 \mu\text{m}$) in which the breakdown current will be correspondingly larger (to be published). For the smaller measurement current, accurate quantisation is observed over a 2 T magnetic field range which is perfectly adequate for primary resistance measurements.

The measurement resolution obtained for most individual measurements of R_{xy}

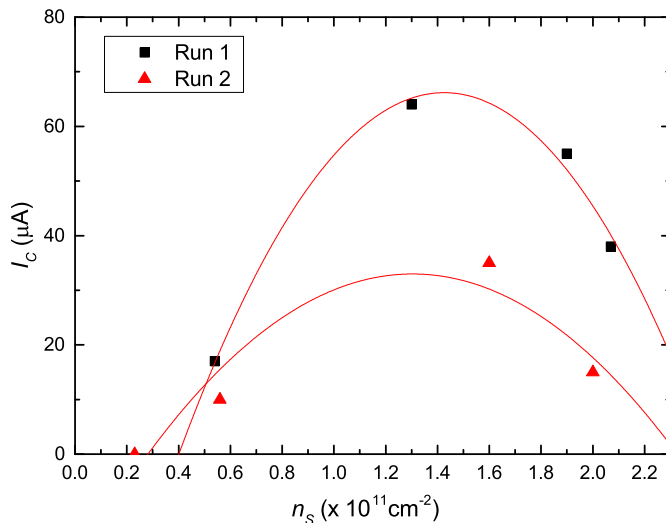


Figure 7. Breakdown current, I_c versus carrier density n_s at $B = 5$ T and $T = 3.9$ K. Black squares are for the first measurement run when the device was new and red triangles are for the second run 3 months later. Red lines are polynomial fits which serves as guide to the eye.

in Fig. 8 is 5 parts in 10^9 for a 15 minute measuring time. A few measurements are made over a longer time (several hours) and are of order 5 part in 10^{10} . This compares very well with traditional QHR systems, especially considering that for the cryogen-free system, there is in principle no limit on the available measurement time.

Figure 9 shows an Allan deviation plot of the measurement resolution for a long measurement run together with results obtained from a previous measurement using our standard quantum Hall system [24]. Both curves show the expected $1/\sqrt{\tau}$ behaviour for uncorrelated white noise. The lower measurement resolution of the cryogen-free system can be explained by the lower measurement current used ($20 \mu\text{A}$ versus $100 \mu\text{A}$) and the higher current noise of the null detector (A20 null-detector versus SQUID null detector), resulting in a factor of 10 difference. For both the cryogen-free system and the traditional system the theoretical optimum measurement resolution is still a factor of 5 better. This is caused by the fact that the noise of CCC-SQUID combination in our systems is about a factor of 5 higher than that of the bare SQUID sensor [24].

6. Summary/Outlook

The results presented here demonstrate that with epitaxial graphene on SiC it is possible to achieve part per billion accuracy in primary resistance metrology using a simple cryogen-free system. Measurements are presented as a function of magnetic field and different source-drain current densities which demonstrate that the operational parameters are sufficiently wide for easy and reliable use. Care has to be taken to adjust

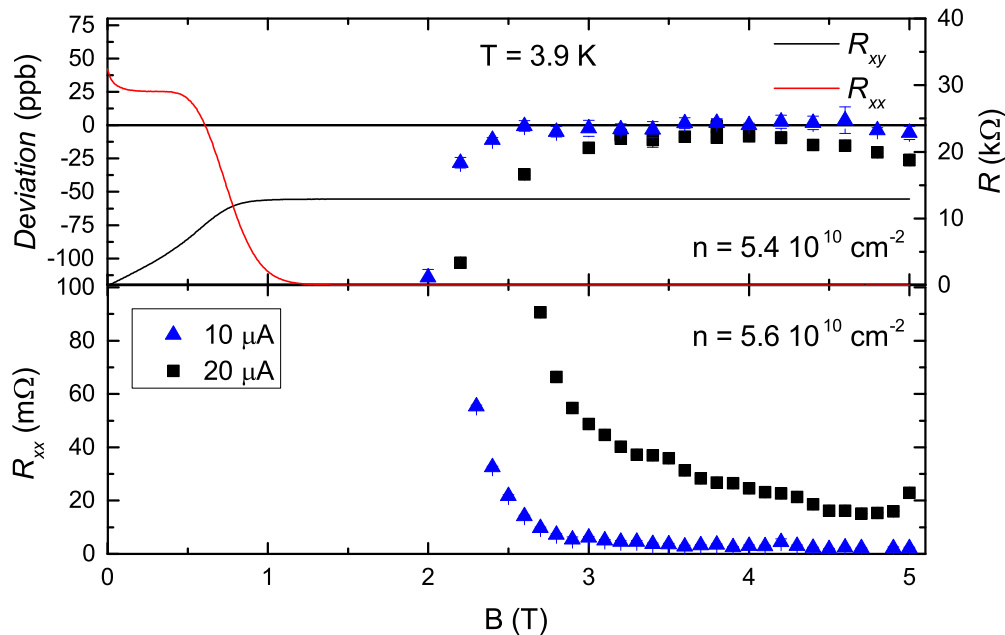


Figure 8. Top panel: R_{xy} (Black) and R_{xx} (Red) as a function of magnetic field measured at a small (100 nA) source-drain current (left axis). Symbols: Measurement of R_{xy} against standard resistor using CCC bridge. The deviation is calculated as a difference from the mean value of the standard resistor in the range of 3 to 4.5 T. Bottom panel: Measurement of R_{xx} over the same magnetic field range for two different measurement currents.

the charge carrier density to the optimum value to ensure a maximum breakdown current density. Corona gating at room temperature and subsequent freezing of the doping is beneficial compared to applying a gate voltage during QHR measurements because no additional noise is injected into the system, but this comes at the expense of the practical inconvenience of thermal cycling the system.

Another practical aspect which needs addressing is the CCC bridge. At the moment this bridge requires a liquid helium dewar to provide the low temperature for the superconducting shield and SQUID. In a separate cryogen-free cryostat we have recently demonstrated that a CCC can be operated in such an environment (to be published). The challenge is to integrate the CCC in the same cryogen-free cryostat as the QHE system and our plan is to do this in the next design iteration of the system.

An alternative to a CCC would be a room temperature comparator bridge. In order to obtain the required ppb-accuracy a large (at least 100 μA) source drain current through the quantum Hall device is needed which is beyond the breakdown current of a single SiC/G device at low magnetic field and high temperature. In a quantum Hall array many devices can be operated in parallel, lowering the resistance value and increasing the total measurement current. The epitaxial graphene needs to be sufficiently homogeneous

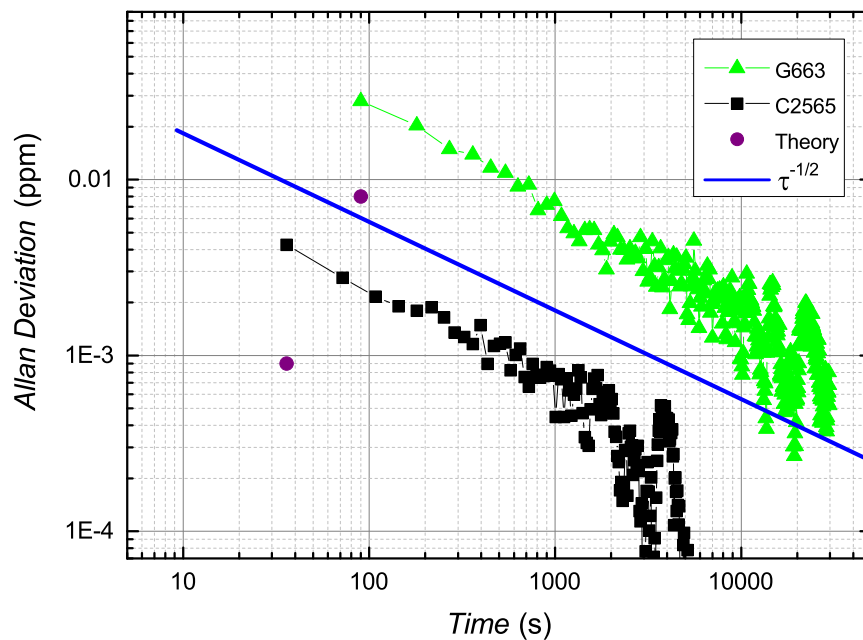


Figure 9. Allan deviation for a long measurement run compared with previously published data in Ref. [24]. Green triangles: Measured using cryogen-free system (5 T and 3.9 K) with a source-drain current of $20 \mu\text{A}$ and a CCC bridge with A20 null detector [23]. Each data point represents a 90 s measurement section composed of three 30 s measurements of either forward or reverse current direction. Black squares: Measured using traditional system with 14 T magnet-300 mK temperature and source-drain current of $100 \mu\text{A}$. The CCC bridge uses a SQUID null detector and each data point represents 30 s of measurement time made up of three blocks of 10 s. Purple dots: Theoretical optimum measurement resolution for each system. Blue line: $1/\sqrt{\tau}$.

so that the operational parameters of all QHR devices overlap and all contacts need to be low ohmic. Recently, the first SiC/G quantum Hall array at $R_K/200$ has been demonstrated [31].

Dissemination and proliferation of primary quantum standards is one of the key objectives of fundamental metrology. The results presented in this paper could be transformative for future resistance metrology by creating the opportunity for many more metrology and calibration laboratories to realise their own primary resistance traceability. This will shorten the calibration chain and lower the uncertainty which can be provided to end users with all its implicit benefits. A number of technical issues remain to be addressed but the basic principle of operation has been demonstrated.

Acknowledgments

This work was supported by the NPL Proof-of-Concept fund, NMS Programme, European Union Seventh Framework Programme under Grant Agreement No. 604391 Graphene Flagship, and EMRP Project GraphOhm.

6.1. References

- [1] See for example the BIPM CMC Website at <http://kcdb.bipm.org>.
- [2] K. v Klitzing, G. Dorda, and M. Pepper. New method for high-accuracy determination of the fine-structure constant based on quantized hall resistance. *Physical Review Letters*, 45(6):4, 1980.
- [3] B. Jeckelmann and B. Jeanneret. The quantum hall effect as an electrical resistance standard. *Measurement Science & Technology*, 14(8):1229–1236, 2003.
- [4] K. S. Novoselov, A. K. Geim, S. V. Morozov, D. Jiang, M. I. Katsnelson, I. V. Grigorieva, S. V. Dubonos, and A. A. Firsov. Two-dimensional gas of massless dirac fermions in graphene. *Nature*, 438(7065):197–200, 2005.
- [5] Y. B. Zhang, Y. W. Tan, H. L. Stormer, and P. Kim. Experimental observation of the quantum hall effect and berry’s phase in graphene. *Nature*, 438(7065):201–204, 2005.
- [6] K. S. Novoselov, Z. Jiang, Y. Zhang, S. V. Morozov, H. L. Stormer, U. Zeitler, J. C. Maan, G. S. Boebinger, P. Kim, and A. K. Geim. Room-temperature quantum hall effect in graphene. *Science*, 315(5817):1379–1379, 2007.
- [7] A. J. M. Giesbers, G. Rietveld, E. Houtzager, U. Zeitler, R. Yang, K. S. Novoselov, A. K. Geim, and J. C. Maan. Quantum resistance metrology in graphene. *Applied Physics Letters*, 93(22):222109–12, 2008.
- [8] A. Tzalenchuk, S. Lara-Avila, A. Kalaboukhov, S. Paolillo, M. Syvajarvi, R. Yakimova, O. Kazakova, T. J. B. M. Janssen, V. Fal’ko, and S. Kubatkin. Towards a quantum resistance standard based on epitaxial graphene. *Nature Nanotechnology*, 5(3):186–189, 2010.
- [9] T. J. B. M. Janssen, N. E. Fletcher, R. Goebel, J. M. Williams, A. Tzalenchuk, R. Yakimova, S. Lara-Avila, S. Kubatkin, and V. I. Fal’ko. Graphene, universality of the quantum hall effect and redefinition of the si system. *New Journal of Physics*, 13:6, 2011.
- [10] A. Satrapinski, S. Novikov, and N. Lebedeva. Precision quantum hall resistance measurement on epitaxial graphene device in low magnetic field. *Applied Physics Letters*, 103(17), 2013.
- [11] C. C. Kalmbach, J. Schurr, F. J. Ahlers, A. Muller, S. Novikov, N. Lebedeva, and A. Satrapinski. Towards a graphene-based quantum impedance standard. *Applied Physics Letters*, 105(7), 2014.
- [12] F. Lafont, R. Ribeiro-Palau, D. Kazazis, A. Michon, O. Couturaud, C. Consejo, T. Chassagne, M. Zielinski, M. Portail, B. Jouault, F. Schopfer, and W. Poirier. Quantum hall resistance standards from graphene grown by chemical vapour deposition on silicon carbide. *Nat Commun*, 6, 2015.
- [13] S. Kopylov, A. Tzalenchuk, S. Kubatkin, and V. I. Fal’ko. Charge transfer between epitaxial graphene and silicon carbide. *Applied Physics Letters*, 97(11):3, 2010.
- [14] S. Tanabe, Y. Sekine, H. Kageshima, M. Nagase, and H. Hibino. Half-integer quantum hall effect in gate-controlled epitaxial graphene devices. *Applied Physics Express*, 3(7):3, 2010.
- [15] S. Lara-Avila, K. Moth-Poulsen, R. Yakimova, T. Bjornholm, V. Fal’ko, A. Tzalenchuk, and S. Kubatkin. Non-volatile photochemical gating of an epitaxial graphene/polymer heterostructure. *Advanced Materials*, 23(7):5, 2011.
- [16] D. Waldmann, J. Jobst, F. Speck, T. Seyller, M. Krieger, and H. B. Weber. Bottom-gated epitaxial graphene. *Nature Materials*, 10(5):357–360, 2011.
- [17] A. Lartsev, T. Yager, T. Bergsten, A. Tzalenchuk, T. J. B. M. Janssen, R. Yakimova, S. Lara-Avila, and S. Kubatkin. Tuning carrier density across dirac point in epitaxial graphene on sic by corona discharge. *Applied Physics Letters*, 105(6), 2014.

- [18] J. Martin, N. Akerman, G. Ulbricht, T. Lohmann, J. H. Smet, K. Von Klitzing, and A. Yacoby. Observation of electron-hole puddles in graphene using a scanning single-electron transistor. *Nature Physics*, 4(2):144–148, 2008.
- [19] J. Huang, J. A. Alexander-Webber, A. M. R. Baker, T. J. B. M. Janssen, A. Tzalenchuk, A. Antonov, T. Yager, S. Lara-Avila, S. Kubatkin, R. Yakimova, and R. J. Nicholas. Disorder induced dirac-point physics in epitaxial graphene from temperature-dependent magneto-transport measurements. *arXiv:1505.03747*, 2015.
- [20] F. Delahaye and B. Jeckelmann. Revised technical guidelines for reliable dc measurements of the quantized hall resistance. *Metrologia*, 40(5):217–223, 2003.
- [21] C. Virojanadara, C Virojanadara, M. Syvajarvi, R. Yakimova, L. I. Johansson, A. A. Zakharov, and T. Balasubramanian. Homogeneous large-area graphene layer growth on 6h-sic(0001). *Physical Review B*, 78(24):6, 2008. R. Yakimova, T. Iakimov, M. Syvjrv, *Process for growth of graphene*, Patent Granted CN 103097283A (2014), 5 pp.
- [22] T. Yager, *et al.*, Low contact resistance in epitaxial graphene devices for quantum metrology. *submitted to AIP Advances*, 2015.
- [23] J. M. Williams, T. J. B. M. Janssen, G. Rietveld, and E. Houtzager. An automated cryogenic current comparator resistance ratio bridge for routine resistance measurements. *Metrologia*, 47(3):167–174, 2010.
- [24] T. J. B. M. Janssen, J. M. Williams, N. E. Fletcher, R. Goebel, A. Tzalenchuk, R. Yakimova, S. Lara-Avila, S. Kubatkin, and V. I. Fal’ko. Precision comparison of the quantum hall effect in graphene and gallium arsenide. *Metrologia*, 49(3):294–306, 2012.
- [25] F. Schopfer and W. Poirier. Quantum resistance standard accuracy close to the zero-dissipation state. *Journal of Applied Physics*, 114(6), 2013.
- [26] X. S. Wu, Y. K. Hu, M. Ruan, N. K. Madiomanana, J. Hankinson, M. Sprinkle, C. Berger, and W. A. de Heer. Half integer quantum hall effect in high mobility single layer epitaxial graphene. *Applied Physics Letters*, 95(22):3, 2009.
- [27] T. Shen, J. J. Gu, M. Xu, Y. Q. Wu, M. L. Bolen, M. A. Capano, L. W. Engel, and P. D. Ye. Observation of quantum-hall effect in gated epitaxial graphene grown on sic (0001). *Applied Physics Letters*, 95(17):3, 2009.
- [28] T. J. B. M. Janssen, A. Tzalenchuk, R. Yakimova, S. Kubatkin, S. Lara-Avila, S. Kopylov, and V. I. Fal’ko. Anomalously strong pinning of the filling factor $\nu = 2$ in epitaxial graphene. *Physical Review B*, 83(23):4, 2011.
- [29] J. A. Alexander-Webber, A. M. R. Baker, T. J. B. M. Janssen, A. Tzalenchuk, S. Lara-Avila, S. Kubatkin, R. Yakimova, B. A. Piot, D. K. Maude, and R. J. Nicholas. Phase space for the breakdown of the quantum hall effect in epitaxial graphene. *Physical Review Letters*, 111(9), 2013.
- [30] B. Jeckelmann and B. Jeanneret. The quantum hall effect as an electrical resistance standard. *Reports on Progress in Physics*, 64(12):1603–1655, 2001.
- [31] A. Lartsev, *et al.*, A prototype of $R_K/200$ quantum hall array resistance standard on epitaxial graphene. *submitted to Journal of Applied Physics*, 2015.